

See discussions, stats, and author profiles for this publication at: <https://www.researchgate.net/publication/229811213>

Incorporation of a Semiconductive Polymer into Mesoporous SBA-15 Platelets: Toward New Luminescent Hybrid Materials

ARTICLE in CHEMISTRY OF MATERIALS · MAY 2011

Impact Factor: 8.35 · DOI: 10.1021/cm103670w

CITATIONS

17

READS

46

7 AUTHORS, INCLUDING:



Fabio Carniato

Amedeo Avogadro University of Eastern Pied...

79 PUBLICATIONS 896 CITATIONS

SEE PROFILE



Silvia Bracco

Università degli Studi di Milano-Bicocca

62 PUBLICATIONS 1,373 CITATIONS

SEE PROFILE



Stefano Caldarelli

Aix-Marseille Université

115 PUBLICATIONS 1,493 CITATIONS

SEE PROFILE



Leonardo Marchese

Amedeo Avogadro University of Eastern Pied...

255 PUBLICATIONS 5,673 CITATIONS

SEE PROFILE


Incorporation of a Semiconductive Polymer into Mesoporous SBA-15 Platelets: Toward New Luminescent Hybrid Materials

Fabio Cucinotta,[†] Fabio Carniato,[†] Geo Paul,[†] Silvia Bracco,[‡] Chiara Bisio,[†] Stefano Caldarelli,[§] and Leonardo Marchese^{*,†}

[†]Dipartimento di Scienze e Tecnologie Avanzate and Nano-SISTEMI Interdisciplinary Centre, Università del Piemonte Orientale “A. Avogadro”, via Teresa Michel 11, I-15121 Alessandria, Italy

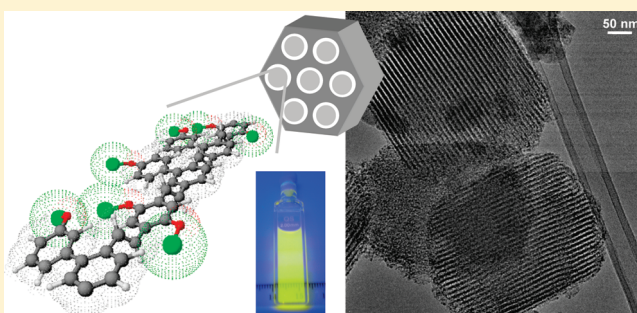
[‡]Department of Materials Science, University of Milano-Bicocca, via R. Cozzi 53, Milan, Italy

[§]Aix Marseille Université, ISM2 UMR 6263, Campus de Saint Jérôme, Service 511 F-13013 Marseille, France

 Supporting Information

ABSTRACT: A polyphenylenevinylene derivative electroluminescent polymer was successfully incorporated into the channels of mesoporous silica SBA-15 with platelet morphology, and the obtained material was fully characterized by mean of X-ray diffraction, nitrogen physisorption porosimetry, infrared spectroscopy, thermogravimetric analysis, scanning electron microscopy (SEM) and high-resolution transmission electron microscopy (HRTEM), solid-state nuclear magnetic resonance (SS-NMR) spectroscopy, ultraviolet–visible (UV–vis) spectroscopy and photoluminescence spectroscopy. The hybrid host–guest system displays significant pore size and volume restriction, along with luminescent properties that mimic those of the polymer in solution, as a consequence of strongly reduced aggregation of the polymer chains when confined in the SBA-15 channels. Moreover, the new composite material possesses a higher photostability than the pure polymer and represents a promising candidate for further use in the field of optoelectronic devices.

KEYWORDS: SBA-15 platelet; mesoporous silica; semiconductive polymer; photoluminescence



INTRODUCTION

Organic optoelectronic devices are becoming commercially important, e.g., in organic light-emitting diodes (OLEDs), organic field-effect transistors (OFETs), and organic solar cells.^{1–7} Light-emitting diodes (LEDs) based on semiconductive polymers are much less expensive to produce than their inorganic counterparts, can be processed even as very thin films in the range of 100 nm of thickness, and render possible the construction of flexible displays. OLEDs can also be operated with low DC voltages and their emissive color can be modulated over the entire visible range by structural modifications.^{6,7}

Although much progress has been made in improving the performance of organic semiconductive polymers, there are still drawbacks associated with the application of these materials, such as reduced fluorescence quantum yields due to molecular aggregation⁸ or the tendency to photobleach in the presence of molecular oxygen.⁹

In order to circumvent these problems and increase both the chemical and thermal stability of organic polymers, the design of hybrid structures containing an inorganic porous host represents a valid solution.¹⁰ Inclusion of dye molecules, nanoparticles, and polymers into microporous and mesoporous materials such as silica, zeolites, etc. is being largely exploited for potential uses in optoelectronic and biosensing devices.^{11–26} In this regard,

ordered mesoporous silicas represent suitable hosts, because of the presence of arrays of uniform nanochannels and/or cages, large pore diameter, high surface area, and optical transparency.^{25–28}

As shown by Tolbert et al., the inclusion of chromophores into nanochannels has been proven to prevent their aggregation and improve the mechanical, thermal, and photochemical stability.¹¹

Furthermore, the works of Corma et al. demonstrated a remarkable increase in the stability of polyphenylenevinylene (PPV) electroluminescent polymer by encapsulation inside the pores of zeolites X and Y.²⁹ Recently, PPV has been also included in a mesoporous metal oxide³⁰ and silica spheres by in situ polymerization and the resulting composite showed highly enhanced optical properties.³¹

However, so far, no other studies have attempted to establish a method whereby the inclusion of such guests can be performed directly from the polymeric form into the mesoporous silica. This would render the material preparation synthetically simpler than employing harsh conditions. Moreover, a host material with tunable morphology and particles size can be exploited to prepare hybrid thin solid films for devices fabrication.

Received: December 24, 2010

Revised: April 8, 2011

Published: May 13, 2011

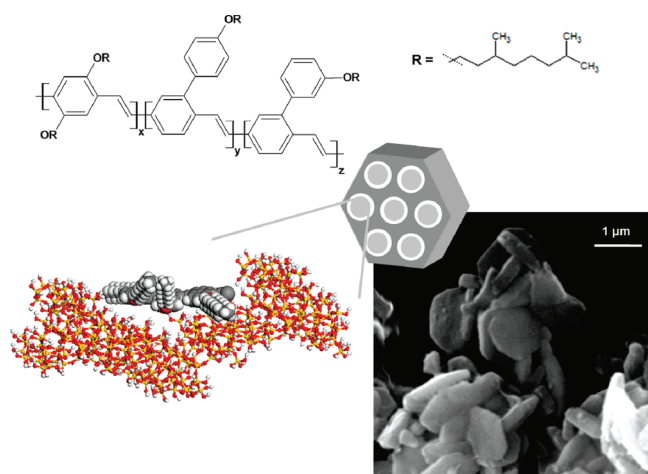


Figure 1. Schematic view of the confinement of Super Yellow polymer (SY) into the nanochannels of SBA-15 platelets.

For these reasons, in this study, we present a new hybrid luminescent system consisting of a semiconductive polymer incorporated into plate-shaped mesoporous silica SBA-15. Through a convenient impregnation process, the silica framework was loaded with an electroluminescent PPV derivative, the Super Yellow copolymer (SY),^{32–35} and the physicochemical behavior of the obtained hybrid material (Figure 1) was investigated. SY showed good processability and electroluminescent performance, because of the presence in the structure of bulky side groups (see Figure 1), which enhance the solubility and reduce the intermolecular interactions that can limit the quantum efficiency.³⁴ In order to further improve and stabilize the emissive properties of SY, we chose, as a hosting framework, the silica-based SBA-15 that has, by far, the largest mesochannels, with thick walls and adjustable pore size ranging from 3 to 30 nm; it also possesses high hydrothermal and mechanical stability, along with the possibility of tailoring its morphology.³⁶ In our study, SBA-15 was prepared as platelet-shaped crystals (Figure 1), following a synthetic methodology reported in the literature,³⁷ in view of possible thin film processing.

EXPERIMENTAL SECTION

Materials. *Platelet SBA-15.* The mesoporous silica crystals with platelet shape were synthesized according to a formerly published procedure.³⁷ Typically, in a 100-mL flask, 1 g of Pluronic P123 triblock copolymer (Aldrich, $M_n = 5800$) was dissolved in 40 g of 2 M HCl aqueous solution and allowed to stir for 3 h at 35 °C. Once the solution became clear, 2.25 mL of TEOS (Aldrich, 98%) and 0.161 g of $\text{ZrOCl}_2 \cdot 8\text{H}_2\text{O}$ (Sigma–Aldrich, 99.5%) were added and the so-formed colloidal suspension was kept stirring at the same temperature for 24 h. Afterward, the gel was transferred to a Teflon vessel, which was sealed and crystallized for further 24 h at 90 °C in an oven under static conditions. The product was filtered, washed with deionized water, and dried in an oven at 80 °C. Prior to use for characterization and guest inclusion experiments, the as-synthesized SBA-15 powder was calcined in air at 500 °C for 12 h, in order to remove the organic template from the pores.

SY/SBA-15. Inclusion of Super Yellow copolymer (SY, from Merck) into the channels of SBA-15 crystals was performed by impregnation from a toluene solution of the polymer. Typically, 200 mg of SBA-15 powder were dispersed in 3 mL of anhydrous toluene and added to a solution of 1 mL of concentrated SY (6 mg mL^{-1} , in toluene). The final

suspension was left stirring at 50 °C under gentle nitrogen stream overnight, until solvent evaporation. The powder was then washed with fresh toluene and filtrated until the washing solution became clear, to ensure that any polymer deposited on the external surface of the SBA-15 crystals was removed.

Characterization Methodologies. X-ray diffraction (XRD) patterns were obtained using an ARL XTRA48 diffractometer with Cu K α radiation ($\lambda = 1.54062 \text{ \AA}$).

High-resolution transmission electron microscopy (HRTEM) micrographs were obtained with a JEOL Model 3010-UHR system that was operating at 300 kV. Samples were ultrasonically dispersed in isopropanol, and a drop of the suspension was deposited on a copper grid covered with a lacey carbon film.

Scanning electron microscopy (SEM) measurements were performed using a LEO 1450 VP instrument. Powder samples were coated with a thin gold layer to ensure surface conductivity.

N_2 physisorption measurements were conducted at liquid nitrogen temperature in the relative pressure from $1 \times 10^{-6}(P/P_0)$ to $1(P/P_0)$, using a Quantachrome Autosorb1MP/TCD instrument. Prior to the analysis, the samples were outgassed at 80 °C for 3 h (residual pressure lower than 10^{-6} Torr). Specific surface areas were determined using the Brunauer–Emmett–Teller (BET) equation, in the relative pressure range from $0.01P/P_0$ to $0.1P/P_0$. The pore size distribution was obtained by applying the nonlocal density functional theory (NLDFT) method.

Infrared spectra of the materials in the form of self-supporting pellets were collected under vacuum conditions (residual pressure $<10^{-5}$ Torr) using a Bruker Model Equinox 55 spectrometer equipped with a pyroelectric detector (DTGS type) with a resolution of 4 cm^{-1} .

All NMR spectra were acquired on a Bruker Model Avance III 500 spectrometer and a wide bore 11.7 T magnet with operational frequencies for ^1H and ^{13}C of 500.13 and 125.77 MHz, respectively. The samples were dehydrated at 80 °C for 2 h before the NMR analysis. A 4-mm triple resonance probe with magic-angle spinning (MAS) was employed in all the experiments. The samples were packed on a ZrO_2 rotor and spun at a MAS rate of 12 kHz. The magnitude of the radio-frequency (RF) field (v_{rf}) was 100 kHz, and the relaxation delay between accumulations was 5 s for ^1H MAS NMR. For the frequency-switched Lee–Goldburg (FSLG) heteronuclear correlation (HETCOR) experiment,³⁸ the sample was packed in a ZrO_2 high-resolution magic-angle spinning (HRMAS) rotor and the volume was restricted to the middle of the rotor. A proton v_{rf} value of 100 kHz was used for FSLG decoupling and during acquisition. A moderate ramped RF field (v_{rfH}) of 62 kHz was used for spin locking, while the ^{13}C RF field (v_{rfC}) was matched to obtain the optimal signal. FSLG HETCOR experiments were recorded with 3k scans, 24 rows, an MAS rate of 12 kHz, and a cross-polarization (CP) contact time of 2 and 5 ms. All chemical shifts are reported using δ scale and are externally referenced to TMS at 0 ppm.

Thermogravimetric analysis (TGA) of the materials was performed under oxygen flow (100 mL min^{-1}) with a SETSYS Evolution TGA-DTA/DSC thermobalance, heating from 50 °C to 800 °C at a rate of $10 \text{ }^\circ\text{C min}^{-1}$.

UV–visible spectra were recorded using a Perkin–Elmer Model Lambda 900 spectrometer. SY and SY/SBA-15 were measured in toluene solution and isopropanol suspension, respectively.

Steady-state emission spectra were recorded on a Horiba Jobin–Yvon Model IBH FL-322 Fluorolog 3 spectrometer equipped with a 450-W xenon arc lamp, double-grating excitation and emission monochromators (2.1 nm/mm dispersion; 1200 grooves/mm), and a Hamamatsu Model R928 photomultiplier tube. Emission and excitation spectra were corrected for source intensity (lamp and grating) and emission spectral response (detector and grating) by standard correction curves. Time-resolved measurements were performed using the time-correlated single-photon counting (TCSPC) option on the Fluorolog 3

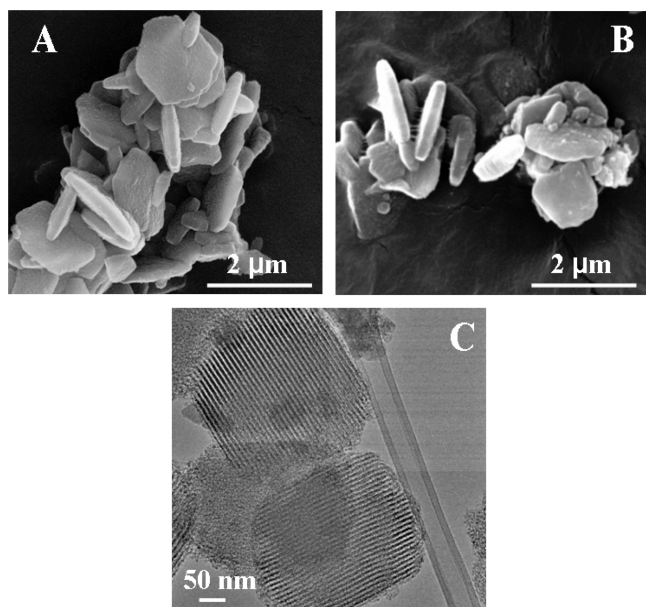


Figure 2. SEM images of (A) SBA-15 and (B) SY/SBA-15; (C) HR-TEM micrograph of the pure silica SBA-15.

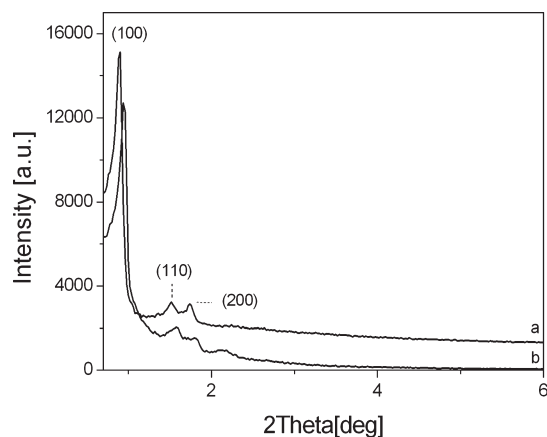


Figure 3. XRD patterns of calcined SBA-15 platelets (curve a) and SY-loaded material (curve b).

spectrometer. A NanoLED (370 nm; full width at half maximum (fwhm) = 1.3 ns) with repetition rates between 10 kHz and 1 MHz was used to excite the sample. The excitation source was mounted directly on the sample chamber at 90° to a double-grating emission monochromator (2.1 nm/mm dispersion; 1200 grooves/mm) and signals were collected using an IBH DataStation Hub photon counting module. Data analysis was performed using the commercially available DAS6 software (Horiba Jobin–Yvon IBH).

RESULTS AND DISCUSSION

The semiconductive PPV derivative (commercial name Super Yellow, abbreviated here as SY) was confined in the channels of SBA-15, as described in the Experimental Section, and its thermal and photophysical properties were improved.

The amount of SY in the final material was estimated to be ~9 wt % using thermogravimetric analysis that was performed under an oxygen flow (see Figure S1 in the Supporting Information).

Table 1. Textural Data (Measured by N₂ Adsorption–Desorption Isotherms) of the Porous Materials

	S_{BET} (m ² /g)	pore volume (cm ³ /g)	pore diameter (Å)
SBA-15	798	1.02	84
SY/SBA-15	587	0.80	75–81

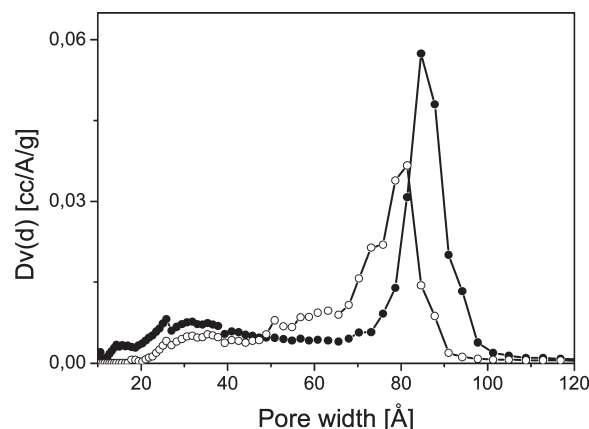


Figure 4. Pore size distribution of (—●—) calcined SBA-15 platelets and (—○—) SY-loaded material.

Morphological, structural, and spectroscopic properties of the host–guest material (hereafter reported as SY/SBA-15) and the pristine SBA-15 were investigated in detail in this work, using a combination of different characterization techniques.

SEM and TEM micrographs of SBA-15 platelet crystals before and after incorporation of the SY polymer are shown in Figure 2. Both solids are composed of interconnected particles with platelet morphology and thickness at the nanometer level (100–200 nm). TEM micrographs of the cross sections of the particles show well-ordered 2D-hexagonal $p6mm$ pore arrangement.

The XRD pattern of pristine SBA-15 platelets (see Figure 3, curve a) shows three distinct reflections: one intense peak at 0.9° 2θ and two weak reflections at 1.5° and 1.7° 2θ , which can be indexed, respectively, as the (100), (110), and (200) planes related to the hexagonal pore array of SBA-15.³⁷ This pattern was also preserved after polymer impregnation (curve b). However, the XRD profile of the hybrid material SY/SBA-15 displays a slight shift to higher 2θ values, which could be assigned to a contraction of the pore diameter,³⁹ confirming that the polymer is incorporated in the silica channels. The impregnation conditions were not critical and did not affect the structural features of the porous silica (see Figure S2 in the Supporting Information).

This interpretation is fully supported by a textural study, which allows one to estimate the surface area (S_{BET} (m²/g)) and pore volume (cm³/g) of the samples. For both the pure silica SBA-15 and the hybrid material, the isotherms are Type IV, according to the IUPAC classification, and have a H1 hysteresis loop, which is representative of mesoporous cylindrical pores (see Figure S3 in the Supporting Information). The results of the nitrogen physisorption isotherms, the BET surface area (S_{BET}), and the total pore volume determined by nonlocal density functional theory (NLDFT) approach,⁴⁰ for pure silica and functionalized material, are shown in Table 1.

SBA-15 possesses high surface area (798 m²/g), a pore volume of 1.02 cm³/g, and a mesopore average diameter of 84 Å.

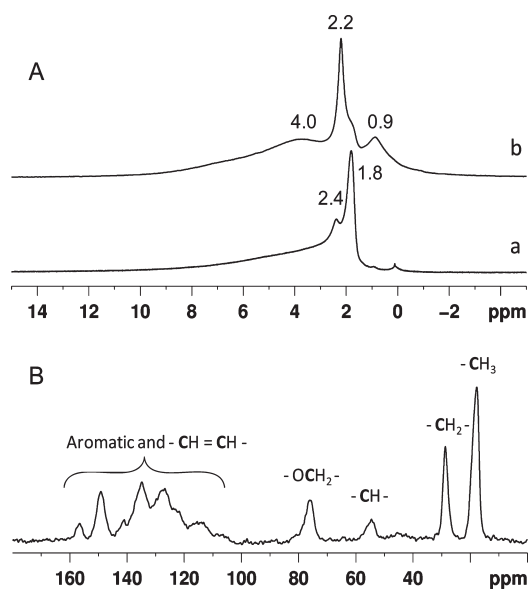


Figure 5. (A) ^1H MAS NMR spectra of dehydrated SBA-15 platelet (curve a) and SY/SBA-15 (curve b), recorded at a MAS rate of 15 kHz. (B) ^{13}C CPMAS NMR spectra of SY/SBA-15 at a MAS rate of 12 kHz and a contact time of 5 ms.

After impregnation with SY, a decrease of both S_{BET} ($587 \text{ m}^2/\text{g}$) and pore volume ($0.80 \text{ cm}^3/\text{g}$) was observed in the final hybrid material (see Table 1). In addition, the pore diameter distribution of SBA-15 broadens and shifts from 84 \AA to ca. $75\text{--}81 \text{ \AA}$ in SY/SBA-15 (Figure 4). These results suggested that the polymer chains are confined into the SBA-15 channels.

The interactions between silica walls and SY were investigated by solid-state NMR (SS-NMR) and infrared spectroscopy.

SS-NMR is well-suited for the investigation of noncovalent interactions in host–guest systems and is a powerful complementary tool to other spectroscopic techniques. Figure 5A displays the ^1H MAS NMR spectra of dehydrated SBA-15 platelets and SY/SBA-15. The SBA-15 spectrum is dominated by the presence of isolated silanols (1.8 ppm)⁴¹ and hydrogen-bonded vicinal silanols (in the range of $3\text{--}7 \text{ ppm}$).⁴² The signal at 2.4 ppm is assigned to silanols weakly interacting with neighboring oxygens.^{43,44}

The ^1H NMR spectrum of SY/SBA15 (Figure 5A, curve b) features detectable signals of the polymer (see Figure S4 in the Supporting Information) at 0.9 ppm (aliphatics) and at $\sim 7 \text{ ppm}$ (broad, aromatics), although the main features are a narrow peak at 2.2 ppm , with a shoulder at 1.8 ppm , and a broad resonance at $\sim 4 \text{ ppm}$. These latter signals are too intense to be assigned to the polymer and, thus, originate from framework silanols. The expected resonance of $-\text{CH}_2\text{O}$ protons at $\sim 3.5 \text{ ppm}$ is likely masked by these more intense signals. The line width of the 2.2 ppm signal suggests that this is stemming from individual silanols, the resonance of which is thus-shifted by the presence of the polymer. Indeed, the presence of a shoulder at 1.8 ppm indicates that a fraction of the framework may not be accessible to the polymer. A downfield shift of the signal of isolated silanols has been observed in zeolites, where it was justified invoking a denser distribution of oxygen nuclei around these specific sites. In the case here reported, the presence of the oxygen and aromatic rings of the polymer may be able to contribute to a shift of the $\text{Si}-\text{OH}$ signal by magnetic susceptibility

or by ring current effects. Finally, the 4 ppm signal, for its position and line width, is tentatively assigned to silanols involved in interactions with the polymer. This assignment is in agreement with IR data (*vide infra*).

Standard CPMAS conditions were used to acquire the ^{13}C NMR spectrum of a dehydrated SY/SBA-15 sample (see Figure 5B). The assignments of the spectral resonances of SY are performed based on ^{13}C solution-state NMR.

To investigate further host–guest arrangements, a CP-based $^1\text{H}-^{13}\text{C}$ HETCOR experiment was performed, with two values of the cross-polarization contact time (Figure 6A). The correlation spectrum recorded with the shorter contact time (2 ms) presents essentially peaks, because of directly bonded proton–carbon pairs. This is the case of the aromatic carbons, the methoxyethylene (which confirms the presence of a peak at 3.5 ppm hidden in the ^1H spectrum) and the aliphatic carbons, with the exception of the low-intensity CH, although the latter with some interesting features. Indeed, while the methyl carbons (18 ppm) correlate with a proton signal at the expected frequency of 0.9 ppm , the CH_2 moieties (29.5 ppm) show a crosspeak with protons at $\sim 2.1 \text{ ppm}$, which is $\sim 1 \text{ ppm}$ downfield, with respect to the values expected for pure SY (see Figure S4 in the Supporting Information) and overlapping with the peak of isolated silanols. Although further studies should be required to clarify this shift, ring current effects stemming from the compression of the chains along the aromatic core of the polymers could be invoked to explain this finding.

To support this hypothesis, correlations between the aromatic carbons and the aliphatic signals are clearly visible even for this short contact time, as a further evidence of close contact between the backbone and the side chains of the polymer. Selective cross correlations between aromatic carbons and methyl protons ($128\text{--}135 \text{ ppm}$, 0.9 ppm) as well as aromatic protons with methyl carbons (7 ppm , 18 ppm) are, in fact, visible.

The correlation spectrum for the longer contact time (5 ms) shows additional peaks among aromatic and aliphatic species, originating by long-distance couplings possibly amplified by spin diffusion in the polymer. Thus, the CH_2O carbon shows correlations to the other aliphatic protons, and the CH_3 and CH_2 carbons to the aromatic ones. The most striking feature of this spectrum, however, is the appearance of correlations between the aromatic carbons and the proton peak at 4 ppm (see Figures 6A and 6B for a more-detailed view), which reinforces the interpretation of this latter signal as being silanols in interaction with aromatic rings, probably by π -electron interactions. The occurrence of this correlation only at longer contact times could be either due to longer C–H distances or to partial residual mobility of the guest. It is thus reasonable to assume a confinement of the SY inside the pores, which reduces its degree of mobility, and leads to interactions between some SiOHs and polymer aromatic rings. Long-contact-time experiments further reveal the presence of guest–guest and host–guest interactions between SY and SBA-15. The latter ones are clearly visible from the cross peaks of SBA-15 and the aliphatic and aromatic moieties of the polymeric chains, confirming the SY confinement and indicating its close proximity to the silica inner walls.

The interaction of the polymer with the silanol groups of the SBA-15 were also detected by infrared spectroscopy, as shown in Figure 7. The intensity of the sharp peak at 3743 cm^{-1} , assigned to the stretching of isolated $\text{Si}-\text{OH}$ groups of the SBA-15, decreases after the impregnation of SY, while the band centered

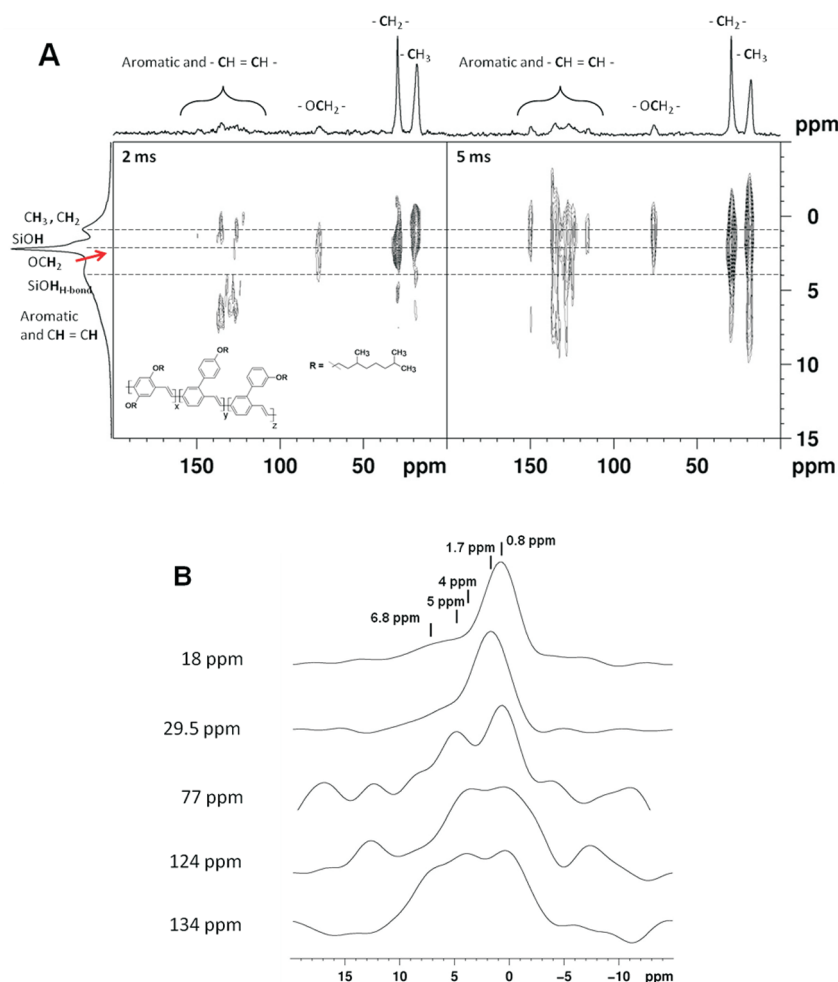


Figure 6. (A) 2D ^1H – ^{13}C FSLG-HETCOR NMR spectra of dehydrated SY/SBA-15 at different contact times, and their corresponding ^{13}C projections and a ^1H MAS spectrum. The data were recorded with 3k scans, 24 rows, and a MAS rate of 12 kHz. (B) Traces from the ^1H – ^{13}C FSLG-HETCOR (contact time = 5 ms) experiments, corresponding to the specified carbon signal.

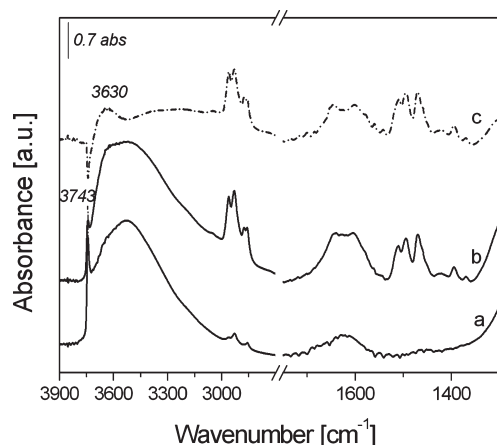


Figure 7. FT-IR spectra of SBA-15 platelets (curve a) and SY/SBA-15 (curve b), recorded under vacuum. Curve c shows the difference spectrum (curve b – curve a).

at 3500 cm^{-1} , which is due to the stretching of Si–OH involved in hydrogen bonds, becomes broader as a consequence of the surface interactions with the polymer side chains.

Such an effect is more clearly illustrated in the difference spectrum (curve b – curve a) shown as curve c in Figure 7, whereby the positive broad band centered at 3630 cm^{-1} is due to the perturbed hydroxyl groups of the silica surface interacting with the π -system of the SY chains.⁴⁴ The shift of vibrational stretching of isolate silanols of ca. 110 cm^{-1} (passing from 3743 to 3630 cm^{-1}) in the final hybrid material matches the data reported in the literature on the interaction studies between silica isolated silanols and aromatic molecules (e.g., benzene).⁴⁵ Interactions between silanol groups and aliphatic moieties of SY are not detectable in this case, because their corresponding signal falls close in frequency to the wide band centered at 3630 cm^{-1} . The features at 3400 – 3000 cm^{-1} cannot be clearly assigned, based on the present results.

Furthermore, the spectrum of SY/SBA-15 shows peaks at high (3060 – 2850 cm^{-1}) and low frequencies (1650 – 1350 cm^{-1}) which can be ascribed, respectively, to the stretching modes of aromatic and aliphatic C–H and to the stretching and bending of C=C and C–H groups typical of the polymeric chains.

A detailed investigation of the photophysical properties of the hybrid material was carried out in comparison to the pristine SY polymer. The outcome reveals a peculiar behavior of SY/SBA-15, in comparison to SY solution and film.⁴⁶

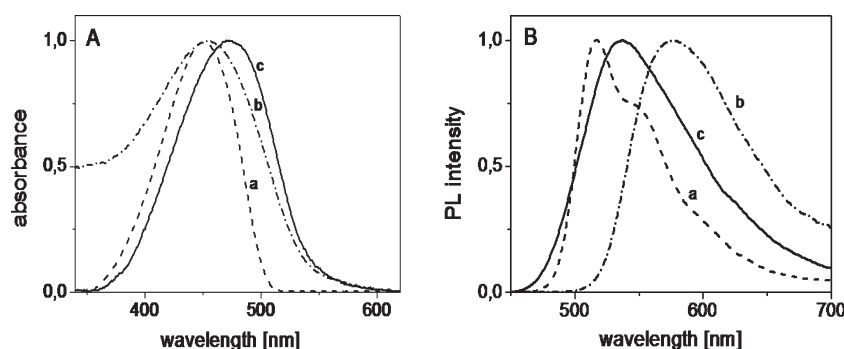


Figure 8. Normalized absorption (A) and emission (B) spectra of a suspension of SY/SBA-15 in isopropanol (curve c), compared to SY in toluene solution (curve a) and in film (curve b). Emission spectra were recorded upon excitation at $\lambda_{\text{exc}} = 430$ nm.

Table 2. Optical Properties of SY Polymer in Toluene Solution and in Film, Compared to SY/SBA-15 in Isopropanol Suspension

	Abs (nm)	PL (nm)	E_g (eV) ^a
SY solution	450	517	2.51
SY film	455	576	2.35
SY/SBA-15	470	536	2.44

^aValues are obtained from the crossing points of absorption and emission spectra.

As shown in Figure 8, both absorption and photoluminescence (PL) spectra of the hybrid system in isopropanol dispersion display red-shifted $\pi^*-\pi$ transitions, with respect to a SY solution. Absorption and emission spectra of SY/SBA-15 were also carried out in other solvents (acetonitrile and dichloromethane), showing no significant differences in the bands position, compared to the measurements performed in isopropanol (see Figure S5 in the Supporting Information). The emission of the composite broadens, peaking at 536 nm, and loses its vibrational structure, indicating that SY emissive and ground states are more distorted to each other than in solution. This effect can be ascribed to aggregation phenomena between the polymer chains within the mesoporous matrix, because the SBA-15 channels are significantly large (big enough to allow such interactions). However, they are strongly reduced, in comparison to a pure polymer film (see also PL excitation spectra in Figure S6 in the Supporting Information), whereby chain aggregation is predominant and the emission undergoes a larger bathochromic shift, being centered at ~ 576 nm. The main optical properties are summarized in Table 2.

In addition, upon incorporation in the SBA-15, the emission lifetime of SY increases to 2.69 ns, from a value of 0.91 ns that was recorded in a toluene solution.

Furthermore, comparing the emission spectra of a diluted SY solution with a SY/SBA-15 suspension that contains an equimolar amount of polymer, the emission intensity from the hybrid composite shows a significant increase (see Figure S7 in the Supporting Information). Moreover, the emission of the hybrid material is less sensitive to the presence of molecular oxygen and water than SY emission (also see Figure S8 in the Supporting Information), as a consequence of a shielding effect played by the SBA-15 channels. In order to further investigate the photostability of the hybrid material, bleaching tests have been performed on dropcasted films and compared with the results obtained from

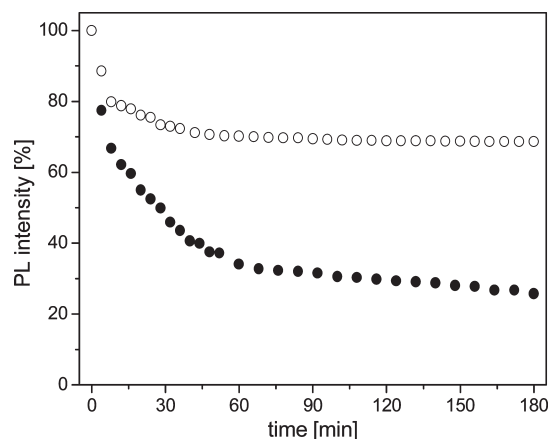


Figure 9. Photoluminescence stability tests, carried out by irradiating (●) a SY film and (○) a SY/SBA-15 film, each at $\lambda_{\text{exc}} = 400$ nm.

a pure organic film (see Figure 9). Photodegradation of SY in SBA-15 is strongly reduced (ca. 70%), with respect to the bleaching that a polymer film undergoes (ca. 25%) after 3 h of light irradiation, confirming that oxygen diffusion into the mesoporous silica is significantly slowed.

CONCLUSIONS

The presented study demonstrates the advantage of employing the mesoporous structure of SBA-15 as host to modulate the physical and chemical properties of electroluminescent polymers.

The new hybrid composite reveals decreased pore volume and size, confirming Super Yellow polymer inclusion, and the luminescence properties are consistent with a reduced aggregation, in comparison to SY film. NMR and IR characterization displays significant host–guest interactions, particularly involving the SBA-15 silanols, with respect to the aliphatic and aromatic moieties of the polymer. The material shows also remarkably increased photostability when compared to pure organic film, which makes the hybrid composite a good candidate for testing and improving the performance of opto-electronic devices.

Further investigations on the composite material are currently being carried out in order to optimize the optical performance and address the study toward the development of novel hybrid light-emitting devices.

■ ASSOCIATED CONTENT

S Supporting Information. Additional information on the physicochemical characterization of the final hybrid material. This material is available free of charge via the Internet at <http://pubs.acs.org>.

■ AUTHOR INFORMATION

Corresponding Author

*Tel: +39 0131 360262. Fax: +39 0131 360250. E-mail: leonardo.marchese@mfu.unipmn.it.

■ ACKNOWLEDGMENT

The financial support of Regione Piemonte (CIPE 2006 Project, "Novel Nanostructured Materials for Light Emitting Devices and Application to Automotive Displays") is gratefully acknowledged. The authors thank Dr. Luca Bertineti for the HRTEM analyses and Dr. Angiolina Comotti for her scientific support in the NMR results interpretation. Authors F. Cucinotta and G. Paul acknowledge Regione Piemonte for a postdoc fellowship. The financial support from "Fondazione Compagnia di San Paolo" for the acquisition of Bruker Avance III 500 SS-NMR spectrometer is gratefully acknowledged.

■ REFERENCES

- (1) Grimsdale, A. C.; Chan, K. L.; Martin, R. E.; Jokisz, P. G.; Holmes, A. B. *Chem. Rev.* **2009**, *109*, 897.
- (2) Sekitani, T.; Someya, T. *Adv. Mater.* **2010**, *22*, 2228.
- (3) Hegelsen, M.; Sondergaard, R.; Krebs, F. C. *J. Mater. Chem.* **2010**, *20*, 36.
- (4) Cheng, Y.-J.; Yang, S.-H.; Hsu, C.-S. *Chem. Rev.* **2009**, *109*, 5868.
- (5) Zhan, X.; Zhu, D. *Polym. Chem.* **2010**, *1*, 409.
- (6) Kamtekar, K. T.; Monkman, A. P.; Bryce, M. R. *Adv. Mater.* **2010**, *22*, 572.
- (7) Mitschke, U.; Bäuerle, P. *J. Mater. Chem.* **2000**, *10*, 1471 and references therein.
- (8) (a) Jakubiak, R.; Collison, C. J.; Wan, W. C.; Rothberg, L. J.; Hsieh, B. R. *J. Phys. Chem. A* **1999**, *103*, 2394. (b) Oelkrug, D.; Tompert, A.; Gierschner, J.; Egelhaaf, H.-J.; Hanack, M.; Hohloch, M.; Steinhuber, E. *J. Phys. Chem. B* **1998**, *102*, 1902.
- (9) (a) Papadimitrakopoulos, F.; Konstantinidis, K.; Miller, T. M.; Opila, R.; Chandross, E. A.; Galvin, M. E. *Chem. Mater.* **1994**, *6*, 1563. (b) Scurlock, R. D.; Wang, B.; Ogilby, P. R.; Sheats, J. R.; Clough, R. L. *J. Am. Chem. Soc.* **1995**, *117*, 10194.
- (10) Angelos, S.; Johansson, E.; Stoddart, J. F.; Zink, J. I. *Adv. Funct. Mater.* **2007**, *17*, 2261.
- (11) Nguyen, T. Q.; Wu, J.; Doan, V.; Schwartz, B. J.; Tolbert, S. H. *Science* **2000**, *288*, 652.
- (12) Chang, Z.; Kevan, L. *Langmuir* **2002**, *18*, 911.
- (13) Lee, K. J.; Oh, J. H.; Kim, Y.; Jang, J. *Adv. Mater.* **2006**, *18*, 2216.
- (14) Hernandez, R.; Franville, A. C.; Minoofar, P.; Dunn, B.; Zink, J. I. *J. Am. Chem. Soc.* **2001**, *123*, 1248.
- (15) Burt, M. C.; Dave, B. C. *J. Am. Chem. Soc.* **2006**, *128*, 11750.
- (16) Robert, G. S.; Forster, R. J.; Keyes, T. E. *J. Phys. Chem. A* **2008**, *112*, 880.
- (17) Zhao, W.; Gu, J.; Zhang, L.; Chen, H.; Shi, J. *J. Am. Chem. Soc.* **2005**, *127*, 8916.
- (18) Carniato, F.; Bisio, C.; Paul, G.; Gatti, G.; Bertineti, L.; Coluccia, S.; Marchese, L. *J. Mater. Chem.* **2010**, *20*, 5504.
- (19) Gao, X.; Nie, S. *J. Phys. Chem. B* **2003**, *107*, 11575.
- (20) Sun, L.-N.; Zhang, H. J.; Peng, C. Y.; Yu, J. B.; Meng, Q. G.; Fu, L. S.; Liu, F. Y.; Guo, X. M. *J. Phys. Chem. B* **2006**, *110*, 7249.
- (21) Gartmann, N.; Brühwiler, D. *Angew. Chem., Int. Ed.* **2009**, *48*, 6354.
- (22) Inagaki, S.; Ohtani, O.; Goto, Y.; Okamoto, K.; Ikai, M.; Yamanaka, K.; Tani, T.; Okada, T. *Angew. Chem., Int. Ed.* **2009**, *48*, 4042.
- (23) Brühwiler, D.; Calzaferri, G.; Torres, T.; Ramm, J. H.; Gartmann, N.; Dieu, L.-Q.; López-Duarte, I.; Martínez-Díaz, M. V. *J. Mater. Chem.* **2009**, *19*, 8040.
- (24) Kim, J.; Piao, Y.; Hyeon, T. *Chem. Soc. Rev.* **2009**, *38*, 372.
- (25) Wirnsberger, G.; Yang, P.; Huang, H. C.; Scott, B.; Deng, T.; Whitesides, G. M.; Chmelka, B. F.; Stucky, G. D. *J. Phys. Chem. B* **2001**, *105*, 6307.
- (26) Scott, B. J.; Bartl, M. H.; Wirnsberger, G.; Stucky, G. D. *J. Phys. Chem. A* **2003**, *107*, 5499.
- (27) Ramamurthy, V. *Photochemistry in Organized and Constrained Media*, VCH: New York, 1991.
- (28) Sen, T.; Jana, S.; Koner, S.; Patra, A. *J. Phys. Chem. C* **2010**, *114*, 707.
- (29) (a) Alvaro, M.; Corma, A.; Ferrer, B.; Galletero, M. S.; García, H.; Peris, E. *Chem. Mater.* **2004**, *16*, 2142. (b) Alvaro, M.; Cabeza, J. F.; Corma, A.; García, H.; Peris, E. *J. Am. Chem. Soc.* **2007**, *129*, 8074.
- (30) Aprile, C.; Teruel, L.; Alvaro, M.; García, H. *J. Am. Chem. Soc.* **2009**, *131*, 1342.
- (31) Kelly, T. L.; Yamada, Y.; Schneider, C.; Yano, K.; Wolf, M. O. *Adv. Funct. Mater.* **2009**, *19*, 3737.
- (32) (a) Gong, X.; Moses, D.; Heeger, A. J.; Liu, S.; Jen, A. K.-Y. *Appl. Phys. Lett.* **2003**, *83*, 183. (b) Becker, H.; Spreitzer, H.; Kreuder, W.; Kluge, E.; Schenk, H.; Parker, I.; Cao, Y. *Adv. Mater.* **2000**, *12*, 42.
- (33) Bolink, H. J.; Coronado, E.; Orozco, J.; Sessolo, M. *Adv. Mater.* **2009**, *21*, 79.
- (34) Spreitzer, H.; Becker, H.; Kluge, E.; Kreuder, W.; Schenk, H.; Demandt, R.; Schoo, H. *Adv. Mater.* **1998**, *10*, 1340.
- (35) Namdas, E. B.; Ledochowitsch, P.; Yuen, J. D.; Moses, D.; Heeger, A. J. *Appl. Phys. Lett.* **2008**, *92*, 183304.
- (36) (a) Zao, D. Y.; Feng, J. P.; Huo, Q. S.; Melosh, N.; Fredrickson, G. H.; Chmelka, B. F.; Stucky, G. D. *Science* **1998**, *279*, 348. (b) Madhugiri, S.; Dalton, A.; Gutierrez, J.; Ferraris, J. P.; Balkus, K. J. *J. Am. Chem. Soc.* **2003**, *125*, 14531.
- (37) Chen, S.-Y.; Tang, C.-Y.; Chuang, W.-T.; Lee, J.-J.; Tsai, Y.-L.; Chan, J. C. C.; Lin, C.-Y.; Liu, Y.-C.; Cheng, S. *Chem. Mater.* **2008**, *20*, 3906.
- (38) (a) Vega, A. J. *J. Am. Chem. Soc.* **1988**, *110*, 1049. (b) Fyfe, C. A.; Zhang, Y.; Aroca, P. *J. Am. Chem. Soc.* **1992**, *114*, 3252. (c) van Rossum, E. J.; Forster, H.; de Groot, H. J. M. *J. Magn. Reson.* **1997**, *124*, 516. (d) Paul, G.; Steuernagel, S.; Koller, H. *Chem. Commun.* **2007**, 5194.
- (39) (a) Gianotti, E.; et al. *Appl. Mater. Interfaces* **2009**, *1* (3), 678–687. (b) Sakthivel, A.; et al. *Microporous Mesoporous Mater.* **2006**, *96*, 293–300.
- (40) (a) Ravikovitch, P. I.; Haller, G. L.; Neimark, A. V. *Adv. Colloid Interface Sci.* **1998**, *76*, 203. (b) Ravikovitch, P. I.; Neimark, A. V. *J. Phys. Chem. B* **2001**, *105*, 6817.
- (41) (a) Grünberg, B.; Emmeler, T.; Gedat, E.; Shenderovich, I.; Findenegg, G. H.; Limbach, H.-H.; Buntkowsky, G. *Chem.—Eur. J.* **2004**, *10*, 5689. (b) Liu, C. C.; Maciel, G. E. *J. Am. Chem. Soc.* **1996**, *118*, 5103.
- (42) (a) Lan, X.; Zhang, W.; Yan, L.; Ding, Y.; Han, X.; Lin, L.; Bao, X. *J. Phys. Chem. C* **2009**, *113*, 6589–6595. (b) Zhang, W. P.; Ratcliffe, C. I.; Moudrakovski, I. L.; Tse, J. S.; Mou, C. Y.; Ripmeester, J. A. *Microporous Mesoporous Mater.* **2005**, *79*, 195.
- (43) Trébosc, J.; Wiench, J. W.; Huh, S.; Lin, V. S.-Y.; Pruski, M. *J. Am. Chem. Soc.* **2005**, *127*, 3057.
- (44) Hartmeyer, G.; Marichal, C.; Lebeau, B.; Rigolet, S.; Caulet, P.; Hernandez, J. *J. Phys. Chem. C* **2007**, *111*, 9066–9071.
- (45) (a) Mauriello, F.; Armandi, M.; Bonelli, B.; Onida, B.; Garrone, E. *J. Phys. Chem. C* **2010**, *114*, 18233. (b) Madathungal, R. R.; Wunder, S. L. *Langmuir* **2010**, *26*, 5077. (c) Garrone, E.; Barbaglia, A.; Onida, B.; Civalieri, B.; Ugliengo, P. *Phys. Chem. Chem. Phys.* **1999**, *1*, 4649. (d) Onida, B.; Allian, M.; Borello, E.; Ugliengo, P.; Garrone, E. *Langmuir* **1997**, *13*, 5107.
- (46) Snedden, E. W.; Cury, L. A.; Bourdakos, K. N.; Monkman, A. P. *Chem. Phys. Lett.* **2010**, *490*, 76.